Physica D 240 (2011) 166–179

Contents lists available at ScienceDirect

Physica D

journal homepage: www.elsevier.com/locate/physd

Capturing eddy shedding in the Gulf of Mexico from Lagrangian observations

Guillaume Vernieres [a,b,*], Christopher K.R.T. Jones [c], Kayo Ide [d]

[a] Science Applications International Corporation, 4600 Powder Mill Road, Beltsville, MD 20705, United States
[b] Global Modeling and Assimilation Office, Mail Code 610.1, Goddard Space Flight Center, Greenbelt, MD 20771, United States
[c] Department of Mathematics, University of North Carolina, Chapel Hill, NC 27599-3250, United States
[d] Department of Atmospheric and Oceanic Science, University of Maryland, College Park, MD 20742-2425, United States

ARTICLE INFO

Article history:
Available online 26 June 2010

Keywords:
Lagrangian data assimilation
Inverse method
Ensemble Kalman filter

ABSTRACT

The nonlinear process of eddy shedding is studied in the context of the Gulf of Mexico. We show that model runs which do not include eddy detachment can reproduce such an event with the assimilation of suitable data obtained from a control run with eddy detachment. This works surprisingly well and with small amounts of data provided the data originates from instruments that are carried by the flow, i.e. Lagrangian. This is compared with analogous assimilation of data from fixed stations which capture the eddy poorly. The remarkable efficacy of Lagrangian data assimilation in this context is explained by considering the structure of the correlation functions and their associated regions of influence.

1. Introduction

Data assimilation endeavors to improve model forecasts and estimates through the systematic incorporation of data. A natural question arises as to how much data is needed, in a given situation, to get certain key features of the model correct. We address this issue in the context of the Gulf of Mexico and in regard to the large eddies that are shed from the Loop Current. These eddies are dominant dynamic features in the Gulf of Mexico. Through an identical twin experiment, we show that relatively small amounts of data can reproduce a detaching eddy in a model run for which the initial data would produce no eddy without data intervention. We show that this works well provided the data comes from instruments that track the eddy, in other words: Lagrangian data. We compare this with an analogous amount of Eulerian data to show the efficacy of using moving instruments when tracking such coherent structures.

The Loop Current is the extension of the Caribbean Current that flows into the Gulf of Mexico (GoM) through the Yucatan Channel. It penetrates the Gulf with varying strength, transporting about 30 Sv [1] and sheds large anticyclonic eddies that propagate westward further into the GoM. It flows as a loop around Cuba and exits the GoM through the Straight of Florida to become the Florida Current, which finally becomes the Gulf Stream at the latitude of Cape Hatteras. The large anticyclonic eddies (400–500 km in diameter) are shed once or twice a year and transport heat westward into the western GoM at speeds of a few kilometers per day. They extend up to 800 m of depth. The Loop Current and its associated warm core eddies are potential sources of energy for hurricanes that would happen to cross over [2]. Eddy shedding is the one and only process that transfers water masses north or south of the Gulf Stream. Warm core eddies are biologically unproductive and are only found north of the jet while cold core eddies are nutrient rich and only found south of the jet. The proper modeling and prediction of these eddies is of utmost importance for fisheries but also ship routing.

The detachment of an eddy in such a flow field is a highly nonlinear event and one of the keys here is to use a data assimilation method that reflects the nonlinearity of the flow field. As a framework, we use the Lagrangian data assimilation method developed by Ide et al. [3] and Kuznetsov et al. [4] in conjunction with the Ensemble Kalman Filter [5–7]. In this formulation, the state vector includes the trajectories of the Lagrangian instruments (drifters or isopycnal floats). We implement a three layer, reduced gravity model of the Gulf of Mexico as it is among the simplest models which captures this critical behavior of eddy shedding. We compare the efficiency of assimilating different types of observations, from the measurement of surface current at fixed stations to surface and isopycnal floats. Our data assimilation experiments consist of: Eulerian data assimilation (EuDA) in which we assimilate velocities at fixed stations; Lagrangian data assimilation of two-dimensional surface drifters (LaDA2d) and finally, the assimilation of three-dimensional isopycnal floats (LaDA3d). We have assimilated three types of observations, namely, the measurement of velocities at fixed station, the horizontal

* Corresponding author at: Global Modeling and Assimilation Office, Mail Code 610.1, Goddard Space Flight Center, Greenbelt, MD 20771, United States.
E-mail addresses: guillaume.vernieres-1@nasa.gov, guillaume.vernieres@gmail.com (G. Vernieres).

0167-2789/$ – see front matter © 2010 Elsevier B.V. All rights reserved.
doi:10.1016/j.physd.2010.06.008

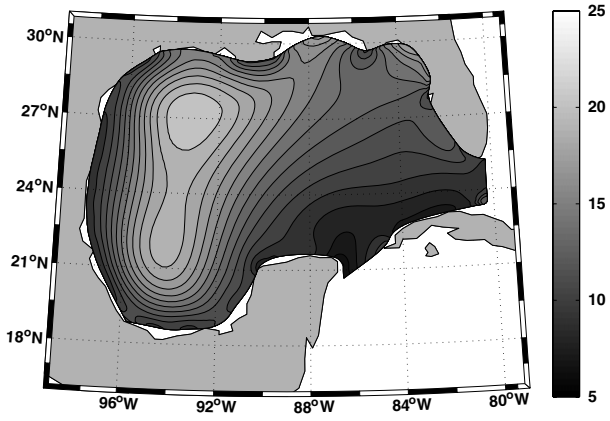

Fig. 1. Resolution of the curvilinear grid. The color scale is in kilometers.

positions of surface drifters, and the three-dimensional positions of isopycnal floats. We show that as few as one judiciously deployed float is sufficient to capture the upper part of an eddy shedding from the Loop Current. We also show that the assimilation of isopycnal floats converges quickly to the control, while the assimilation of the velocities at a limited number of fixed stations estimates the eddy poorly. The remarkable efficiency of the assimilation using Lagrangian data is explained by looking at the structure of the correlation functions and their associated region of influence. The properties of the dynamically estimated correlation functions are used to investigate the efficiency of assimilating the three types of observations used in this study.

We first describe the model and the assimilation method in Sections 2 and 3. The experimental set-up and the results are described in Sections 3 and 4. Section 5 describes the structure of the dynamically estimated correlation functions. A discussion in Section 6 concludes the paper.

2. Model description

We have implemented a multi-layer reduced gravity model of the Gulf of Mexico (GoM). This modeling set-up has been shown to be the simplest representation of the GoM that simulates the shedding of eddies [8]. The model equations, extended with the drifter equations, are:

$$\frac{\mathrm{d}\mathbf{u}^{(j)}}{\mathrm{d}t} + \mathbf{k} \times f\mathbf{u}^{(j)} = \frac{1}{\rho_0}\nabla P^{(j)} + A_h \nabla^2 \mathbf{u}^{(j)} \tag{1}$$

$$\frac{\partial h^{(j)}}{\partial t} + \nabla \cdot (\mathbf{u}^{(j)} h^{(j)}) = 0 \tag{2}$$

$$\frac{\mathrm{d}}{\mathrm{d}t}\mathbf{x}_D{}^{(i)} = \mathbf{u}^{(1)}(\mathbf{x}_D{}^{(i)}(t), t) \quad i = 1, \ldots, N_D \tag{3}$$

where $j = 1, \ldots, N_l$ represents the layer indexing, layer 1 is at the top and N_l at the bottom, $\mathbf{u}^{(j)}$ is the vertically averaged velocity of layer j, $h^{(j)}$ is the thickness of layer j, $\mathbf{x}_D{}^{(i)}$ represents the horizontal position of the drifter i, N_D is the number of drifters, $\mathbf{k}$ is the basis vector representing the vertical direction, $A_h = 400\ \mathrm{m^2\ s^{-1}}$ is a diffusion coefficient, $\rho_0 = 1026\ \mathrm{kg\ m^{-3}}$ is the average density and $g' = 0.29 \times 10^{-3}\ \mathrm{m\ s^{-2}}$ is the reduced gravity.

In this study, we use a three-layer model ($N_l = 3$), the Montgomery potential $P^{(j)}$ of layer j in (1) is then given by

$$P^{(1)} = \rho_0 g'(3h^{(1)} + 2h^{(2)} + h^{(3)}) \tag{4}$$

$$P^{(2)} = \rho_0 g'(2h^{(1)} + 2h^{(2)} + h^{(3)}) \tag{5}$$

$$P^{(3)} = \rho_0 g'(h^{(1)} + h^{(2)} + h^{(3)}) \tag{6}$$

where we have assumed that the difference in density between two consecutive layer is $3\ \mathrm{kg\ m^{-3}}$.

The model uses a structured curvilinear grid in the horizontal, created by the use of elliptic grid generation techniques [9,10]. The variable horizontal resolution has a minimum of about 5 km in the region of the Loop Current. This configuration allows us to reduce the number of degrees of freedom to a minimum without sacrificing grid points to land-masking. The time step is set to 300 s, which gives a velocity based CFL number of 0.12 [11] at the location of the smallest grid size. This small number is required to avoid the instabilities introduced by the noisy Jacobian of the curvilinear grid [10]. The boundary of the grid, illustrated in Fig. 1, follows the coastline. The Eqs. (1) and (2) are discretized using second order finite differences [12], and numerical noise is filtered using a fourth order Laplacian operator as in [13].

The circulation in the GoM is forced by a steady inflow–outflow transport. We impose a cosine shaped current at the Yucatan Channel and the Strait of Florida with widths of 160 km and 150 km respectively and a total transport of 30 Sv as indicated in [14]. In order to conserve the total mass in the Gulf, the inflow transport matches the outflow transport. As in [8], the current is confined to the upper two layers with the top layer carrying two-thirds of the total volume transport.

3. Assimilation of drifter trajectories

We follow the Lagrangian data assimilation (LaDA) method developed by Ide et al. [3] for the assimilation of the drifter trajectories. The method was originally developed based on the extended Kalman filter and has been applied to ocean data assimilation using the ensemble Kalman filter [15,16]. For consistency, the notation closely follows a standard proposed by Ide et al. [17].

The model state is augmented with the zonal and meridional locations of the drifters. We write the augmented state vector as:

$$\mathbf{x}^T = [\mathbf{x}_F^T \quad \mathbf{x}_D^T] \tag{7}$$

where $\mathbf{x}_D$ is in $\mathbb{R}^L$ and contains the two-dimensional coordinates of the drifter location $\mathbf{x}_D^{(i)}$. $L = 2N_D$ is the total number of observations. The vector $\mathbf{x}_F$ is in $\mathbb{R}^N$ and contains the prognostic variables $u^{(j)}$, $v^{(j)}$ and $h^{(j)}$ at each of the grid points.

The semi-discrete (discrete in space, continuous in time) form of the augmented model equations are:

$$\frac{\mathrm{d}\mathbf{x}}{\mathrm{d}t} = \frac{\mathrm{d}}{\mathrm{d}t}\begin{pmatrix}\mathbf{x}_F \\ \mathbf{x}_D\end{pmatrix} = \begin{pmatrix}\mathbf{m}_F(\mathbf{x}_F, t) \\ \mathbf{m}_D(\mathbf{x}_D, \mathbf{x}_F, t)\end{pmatrix} = \mathbf{m}(\mathbf{x}, t) \tag{8}$$

where $\mathbf{m}_F \in \mathbb{R}^N$ is the nonlinear operator corresponding to the discretized version of the layered model (1) and (2) while $\mathbf{m}_D \in \mathbb{R}^L$ is the operator corresponding to the drifter equation (3). We have hidden the complexity of the observing system in the augmented model equation. If we were to use the variational method, the complexity would have been shifted to the model equation and the adjoint models of the nonlinear operators $\mathbf{m}_F$ and $\mathbf{m}_D$ would have needed to be implemented. In contrast, the ensemble filtering approach does not require such a derivation.

The observation $\mathbf{y} \in \mathbb{R}^L$ is related to $\mathbf{x}$ by,

$$\mathbf{y} = \mathbf{H}\mathbf{x} \tag{9}$$

where $\mathbf{H}$ is the observation operator. For the assimilation of only Lagrangian data, $\mathbf{H}$ is simply

$$\mathbf{H} = [\,\mathbf{0} \quad \mathbf{I}\,] \tag{10}$$

where $\mathbf{0}$ is in $\mathbb{R}^{L\times N}$, $\mathbf{I}$ is in $\mathbb{R}^{L\times L}$. The actual observation $\mathbf{y^o}$ is often assumed to have additive Gaussian noise,

$$\mathbf{y^o} = \mathbf{H}\mathbf{x}^t + \boldsymbol{\epsilon} \tag{11}$$

where $\mathbf{x}^t$ is the unknown true state of the ocean and $\boldsymbol{\epsilon}$ is a random noise with covariance $\mathbf{R}$.

Most of the sequential data assimilation methods regress the difference between the analysis and the forecast onto a basis of the data space. The elements of the basis are constructed from the projection of a proxy of the model error covariance onto the data space. The best linear unbiased estimate is written as:

$$\mathbf{x}_j^a - \mathbf{x}_j^f = \sum_{i=1}^{L} \beta_j^{(i)} \mathbf{r}^{(i)} \tag{12}$$

where $\mathbf{x}_j^a$ and $\mathbf{x}_j^f$ are analysis and forecast of the j-th ensemble member, for $j = 1, \ldots, N_e$, $\beta_j^{(i)} \in \mathbb{R}$ is the regression coefficient of the i-th observation, for $i = 1, \ldots, L$, and $\mathbf{r}_i \in \mathbb{R}^{N+L}$ $i = 1, \ldots, L$ is a representer [18,6,19,20].

Each of the representer vectors $\mathbf{r}_i$ correspond to the covariance between the model's state $\mathbf{x}^f$ and its projection onto the observation space $\mathbf{y}^f = \mathbf{H}\mathbf{x}^f$. The representers $\mathbf{r}_i$ are constructed using an ensemble based method. Following Evensen [7], we construct the model error covariance matrix $\mathbf{P}^f$ at time t from an ensemble of model forecasts. Since the true state is unknown, $\mathbf{P}^f$ is computed around the mean of the ensemble $\overline{\mathbf{x}^f}$. We write:

$$\mathbf{P}^f \approx \mathbf{P}_e^f = \frac{1}{N_e - 1}\sum_{j=1}^{N_e}(\mathbf{x}_j^f - \overline{\mathbf{x}^f})(\mathbf{x}_j^f - \overline{\mathbf{x}^f})^T \tag{13}$$

where N_e is the size of the ensemble. The i-th column of the matrix $\mathbf{P}_e^f\mathbf{H}^T$ corresponds to the representer vector $\mathbf{r}_i$,

$$\mathbf{P}_e^f\mathbf{H}^T = \frac{1}{N_e - 1}\sum_{j=1}^{N_e}(\mathbf{x}_j^f - \overline{\mathbf{x}^f})(\mathbf{y}_j^f - \overline{\mathbf{y}^f})^T \tag{14}$$

where $\overline{\mathbf{y}^f}$ is the mean of $\mathbf{y}_j^f$.

For LaDA, following Salman et al. [15,16], we decompose the error covariance matrix into:

$$\mathbf{P}_e^f = \begin{pmatrix}\mathbf{P}_{FF}^f & \mathbf{P}_{FD}^f \\ \mathbf{P}_{DF}^f & \mathbf{P}_{DD}^f\end{pmatrix} \tag{15}$$

and thus, the projection of $\mathbf{P}_e^f$ onto the data space is:

$$\mathbf{P}_e^f\mathbf{H}^T = \begin{pmatrix}\mathbf{P}_{FD}^f \\ \mathbf{P}_{DD}^f\end{pmatrix}. \tag{16}$$

The regression coefficients $\boldsymbol{\beta}_j = [\beta_j^{(1)}, \ldots, \beta_j^L]^T$ in (12) are determined by,

$$\boldsymbol{\beta}_j = (\mathbf{P}_{DD}^f + \mathbf{R})^{-1}\mathbf{d}_j \tag{17}$$

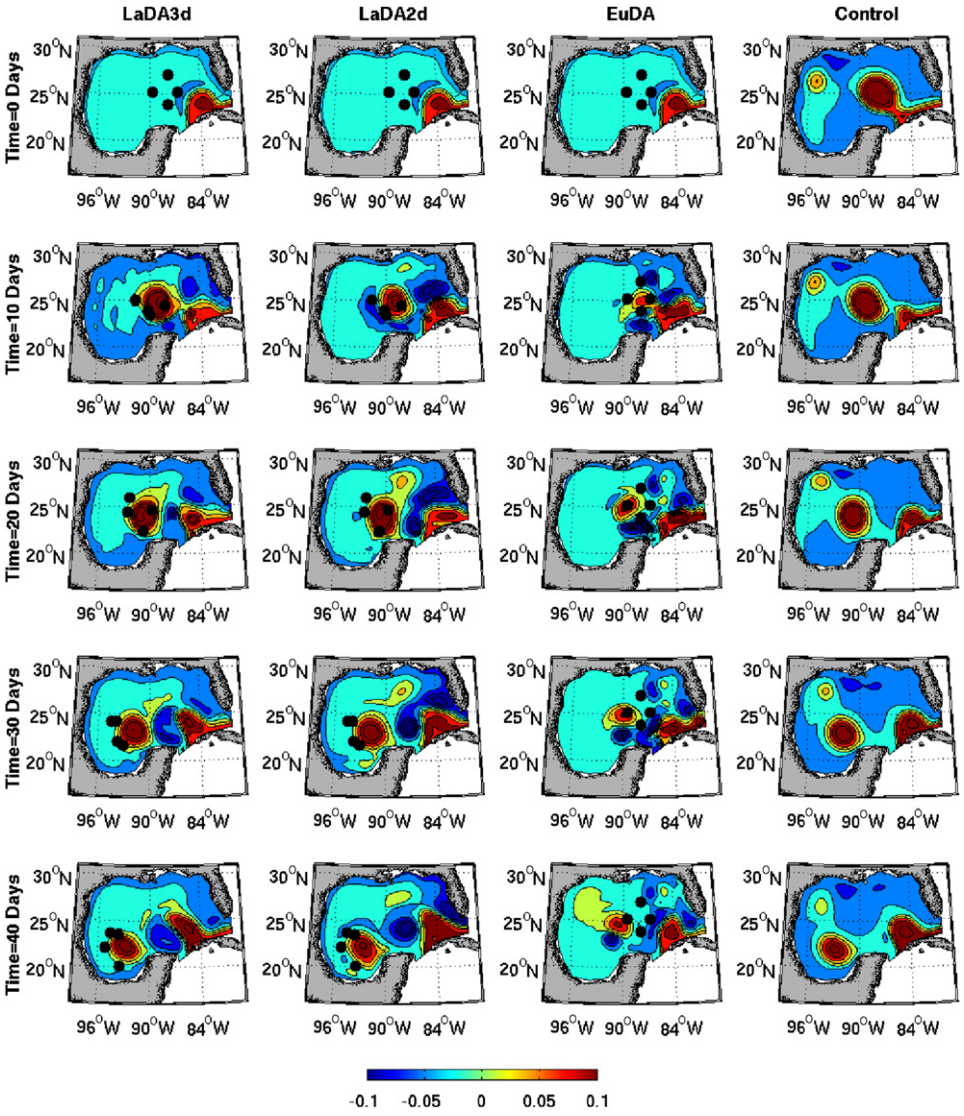

Fig. 2. The SSH field in meters. From left most column to right most column: Analysis from LaDA3d, analysis from LaDA2d, analysis from EuDA and control.

where $j = 1, \ldots, N_e$ is the ensemble index and $\mathbf{d}_j$ is the innovation vector for the ensemble j at time t. We write,

$$\mathbf{d}_j = \mathbf{y}^{\mathbf{o}} - \mathbf{H}\mathbf{x}_j^f + \tilde{\boldsymbol{\epsilon}}_j \tag{18}$$

where $\tilde{\boldsymbol{\epsilon}}_j$ is drawn from a Gaussian distribution with covariance $\mathbf{R}$, to circumvent the problem of generating an analysis ensemble that has a variance that is too low [21].

4. Experimental set-up

This section describes the experimental set-up using the perfect model scenario in which the control (truth) is generated by the same model as the data assimilation system, and the synthetic observations are sampled from the control. We first describe the control experiment of choice. The control experiment is also used to evaluate the results of the data assimilation. The details of the ensemble initialization and localization are discussed at the end of the section.

4.1. Control experiment

The initial condition for the control is obtained by integrating the model from a resting state for 400 days. The control run of choice is depicted in the rightmost column of Fig. 2 for 50 days, by the sea surface height (SSH) field. It shows the eddy shedding from the Loop Current, followed by its westward propagation with an average phase speed of 15 km/day. Therefore, there are two aspects to this set-up for the evaluation of the different data assimilation systems. One is the estimation of the eddy-shedding process and the other is the estimation of the eddy-propagation process. This physical phenomenon is typical of the GoM and has been extensively studied (see, for example, a recent study by Yin and Oey [22]).

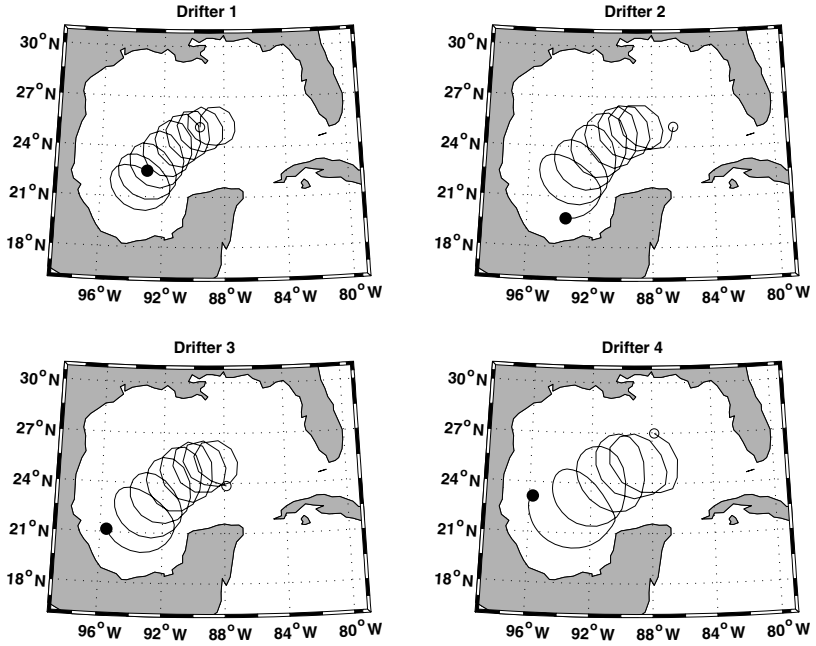

Fig. 3. Horizontal trajectories of the 4 synthetic drifters. The time span is 50 days.

4.2. Synthetic observations

We assimilate three types of observations sampled from the control over a period of 50 days. The first type is Eulerian (EuDA) and corresponds to the observation of surface velocities at fixed stations. We use a realistic sampling rate set to one hour. In our setting, these surface velocities are extracted from the control run's top layer at the four station positions, where the linear observation operator **H** in (9) corresponds to the bi-cubic spatial interpolation. The observation are obtained by adding Gaussian noise to the true velocity of the control

$$\mathbf{y^o}(t) = [u_t^{(1)}(x_1, y_1, t) \quad v_t^{(1)}(x_1, y_1, t) \quad \cdots \quad u_t^{(1)}(x_4, y_4, t) \quad v_t^{(1)}(x_4, y_4, t)]^T + \boldsymbol{\epsilon}_u \tag{19}$$

where $u_t^{(1)}(x_l, y_l, t)$ and $v_t^{(1)}(x_l, y_l, t)$ are the two-dimensional velocity at the l-th station and the standard deviation of the measurement error $\|\boldsymbol{\epsilon}_u\|$ is set to 10^{-2} m/s. We have assumed that measurement errors of the zonal and meridional velocities and the different stations are uncorrelated. Using a set of Eulerian observations taken at the station positions in the real GoM, the EuDA resulted in poor performance at reproducing the eddy-shedding process, and thus also the eddy-propagation process that should have followed. The set of station positions used in this study is depicted in Fig. 2. This set can extract more information about the eddy-shedding process and results in better performance than the real set of station positions.

We also assimilate two types of Lagrangian observations. The first type is the surface drifter that observes the horizontal (two-dimensional) positions. We call this data assimilation system LaDA2d. For the purpose of eddy tracking, four drifters are deployed in the eddy, initially in the control flow. The trajectories of four drifters orbiting around the eddy center are depicted in Fig. 3. These trajectories are observed at the sampling rate of 12 h for 50 days. Although surface drifters can communicate their location more frequently, we use a coarse sampling rate to demonstrate the robustness of the LaDA method. Like velocity observations, Lagrangian observations are subject to error

$$\mathbf{y^o}(t) = \mathbf{x}_D^t + \boldsymbol{\epsilon}_{xy} \tag{20}$$

where the standard deviation of the measurement error $\boldsymbol{\epsilon}_{xy}$ is set to 300 m. Similarly, as in the EuDA case, we assume that measurement errors of the zonal and meridional positions and between drifters are uncorrelated.

The second type of Lagrangian data correspond to that coming from isopycnal floats. We assume that isopycnal floats move with the flow at the bottom of the top layer and observe the horizontal and vertical (3D) position. This system is referred to as LaDA3d. In this case, the linear observation operator **H** in (9) corresponds to not only the location of the isopycnal float as in the LaDA2d case, but also the top layer thickness $h^{(1)}(\mathbf{x}_D^{t\,(1)}, \mathbf{x}_D^{t\,(2)}), \ldots, h^{(1)}(\mathbf{x}_D^{t\,(7)}, \mathbf{x}_D^{t\,(8)})$ at the position of the float [23,24].

$$\mathbf{y^o}(t) = [\,\mathbf{x}_D^t \quad h^{(1)}(\mathbf{x}_D^{t\,(1)}, \mathbf{x}_D^{t\,(2)}) \cdots h^{(1)}(\mathbf{x}_D^{t\,(7)}, \mathbf{x}_D^{t\,(8)})\,]^T + [\,\boldsymbol{\epsilon}_{xy}^T \quad \boldsymbol{\epsilon}_z^T\,]^T \tag{21}$$

where the standard deviation of $\boldsymbol{\epsilon}_z$ is set to 1 m.

We have assumed that the isopycnal floats communicate their positions (including depth) every 12 h. The error resulting from the communication method (sound triangulation, or surfacing to broadcast the observations to a satellite) is included in the assumed measurement and representation error. An example of the three-dimensional trajectory of an isopycnal drifter is depicted in Fig. 4. Since the flow is vertically uniform within each layer, and the horizontal velocities are a few orders of magnitude larger than the vertical velocities, the horizontal trajectories are the same than the ones depicted in Fig. 3. Carter [23] and Mead and Bennett [24] also assimilated the isopycnal float observations in a shallow water model. However they converted the positions into Eulerian velocities.

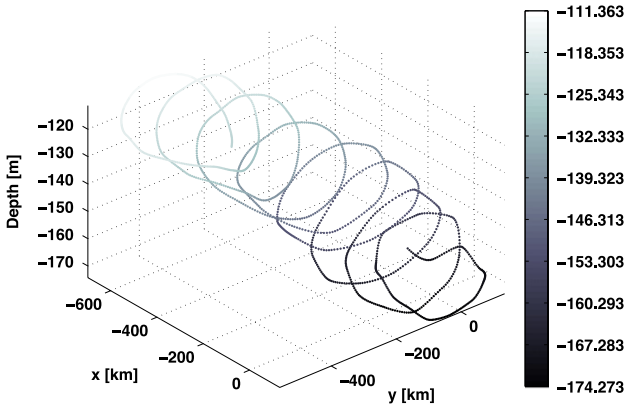

Fig. 4. Three-dimensional trajectory of an isopycnal float. The initial position of this float corresponds to the initial position of drifter 1 from Fig. 3.

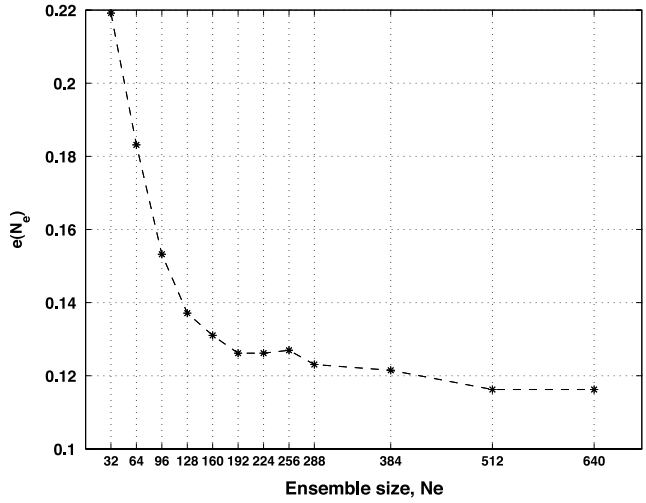

Fig. 5. Convergence of the correlation functions after 5 days of assimilation.

4.3. Ensemble initialization

In this idealized experiment, we only consider errors in the initial field, neglecting the dynamical and boundary errors. For each members, the initial condition for the layer thicknesses is created by adding 900 Gaussian shaped perturbations to a prior estimate of the initial condition corresponding to the GoM circulation with no eddy present. The decorrelation length scale is set to 50 km and the magnitude of each of the Gaussian shaped perturbations is drawn from a uniform distribution on [−7 m 7 m] while the decorrelation length scale is set to 50 km. The velocities are not perturbed.

The perturbations are the same for the three active layers. The initial ensemble for the surface drifter location is created by perturbing the initial horizontal position of the drifters using a uniform distribution on [−200 m 200 m]. The initial ensemble for the horizontal position of the isopycnal floats is perturbed the same way, the vertical position is perturbed using a uniform distribution in [−1 m 1 m].

4.4. Ensemble size, localization and filtering

The computation of the ensemble is parallelized on 128 cpu's of the Topsail cluster at UNC. The parallelization method is similar to the one described in [25]. We can run experiments ranging from 32 to 1280 members i.e., $N_e = 32, 64, 96, 128, 160, 192, 224, 256, 288, 384, 512, 640$ and 1280. This permits us to study the convergence of the representers: $\mathbf{P}^f_e\mathbf{H}^T$. We define the error $e(N_e)$ in the correlation function as a function of the ensemble size N_e by,

$$e(N_e) = \|\mathbf{C}^f_{FD}(N_e) - \mathbf{C}^f_{FD}(1280)\| \tag{22}$$

where $\|.\|$ is the entrywise Frobenius norm of a matrix. The ijth element of the correlation matrix projected on the data space is defined by

$$(\mathbf{C}^f_{FD})^{ij} = \frac{(\mathbf{P}^f_{FD})^{ij}}{\sqrt{(\mathbf{P}^f_{FF})^{ii}}\sqrt{(\mathbf{P}^f_{DD})^{jj}}} \tag{23}$$

where $\mathbf{x}^f_D$ is the meridional and zonal position of a surface drifter, $\sqrt{(\mathbf{P}^f_{FF})^{ii}}\left(\sqrt{(\mathbf{P}^f_{DD})^{jj}}\right)$ is the standard deviation of the ith (jth) component of the state vector (observation vector), calculated from the ensemble.

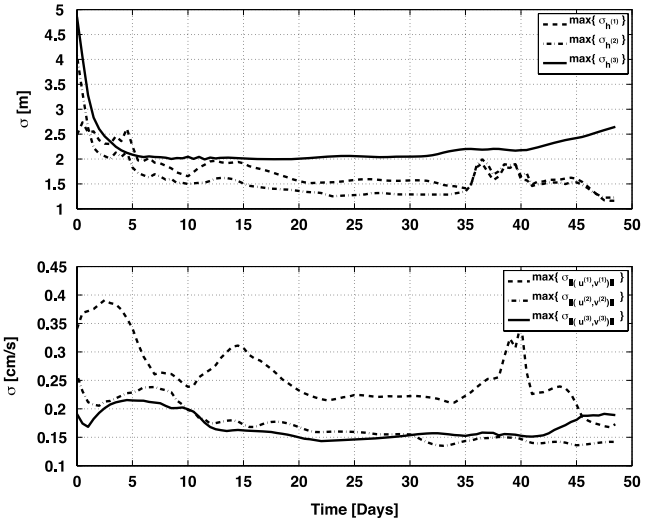

Fig. 6. Ensemble spread. The top panel is the maximum standard deviation of the layer thickness for the three layers. The bottom panel is the maximum standard deviation of the horizontal velocities.

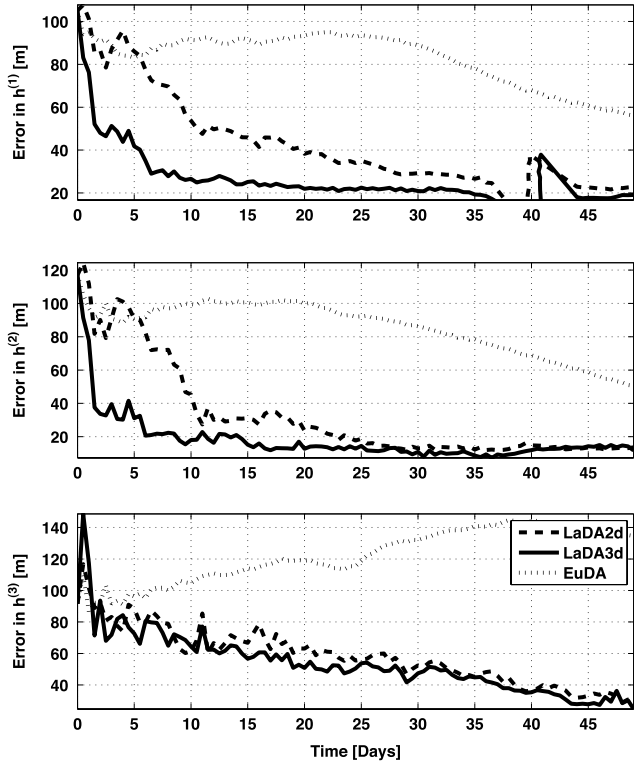

Fig. 7. The RMS of the layer thickness between the truth and the analysis. The RMS is computed in a 250 km radius around the eddy for the first layer (top), the second layer (middle), and the third layer (bottom).

Fig. 5 depicts the convergence of $e(N_e)$ after 5 days of assimilation, with the localization radius set to infinity for the LaDA2d case. It shows that a reasonable convergence is achieved for an ensemble size of 256 or more. This is by no mean a proof that the estimated representers have converged to the true representers. Study of the representer field, far away from the location of the observations, showed significant spurious correlation in the case of 1280 members. The results presented in the next section use an ensemble size of 256 members.

In the next section, the far field spurious correlations are filtered out using a localization radius of 300 km. The localization method follows [26], (23) becomes,

$$(\mathbf{C}^f_{FD})^{ij} = \mathbf{S} \circ \frac{(\mathbf{P}^f_{FD})^{ij}}{\sqrt{(\mathbf{P}^f_{FF})^{ii}}\sqrt{(\mathbf{P}^f_{DD})^{jj}}} \tag{24}$$

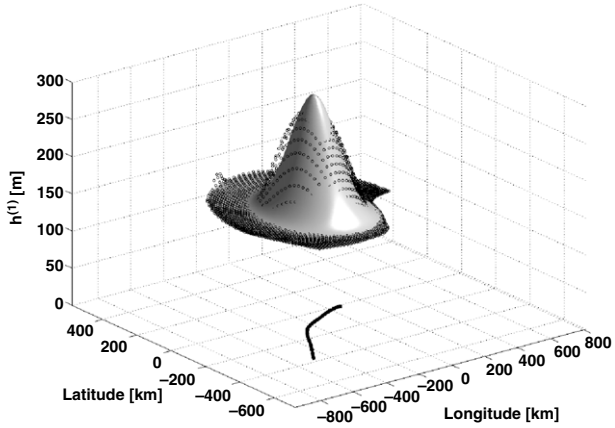

Fig. 8. Trajectory of the eddy (thick black line) for the first 43 days and snapshot of the Gaussian function (shaded surface) at $t = 43$ days with parameters ($\alpha = -480$ km, $\beta = -378$ km, $B = 198$ m, $A = 158$ m, $L = 144$ km). The black circles represent a snapshot of the top layer from the truth a the same time.

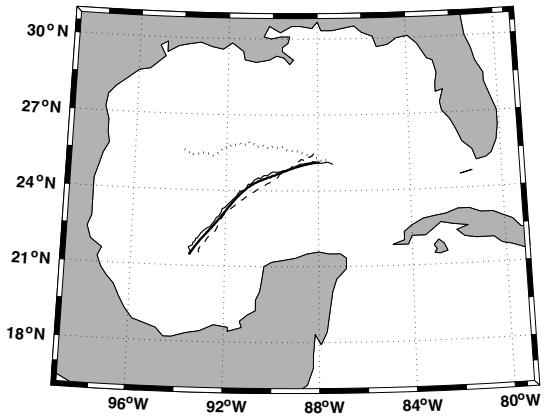

Fig. 9. Trajectory of the eddy; LaDA2d (thin solid), LaDA3d (dashed), EuDA (dotted), and truth (thick solid).

where $\mathbf{S} \circ \mathbf{B}$ denotes the Schur product of a matrix $\mathbf{S}$ with a matrix $\mathbf{B}$. The element $S_{i,j}$ is obtained from the correlation function ϱ applied to the distance in $\mathcal{R}^2$, where

$$\varrho(r) = \exp\left(-\frac{r^2}{2r_o^2}\right) \tag{25}$$

where r_0 is the localization radius and r is the distance from the observation.

The initial ensemble and the data assimilation steps introduce spurious temporal and spatial oscillations as well as sharp gradients that are filtered in the following way:

$$\langle \mathbf{x}_j^a(t) \rangle = \frac{1}{3}(\langle \mathbf{x}_j^a(t-\delta) \rangle + \mathbf{x}_j^a(t) + \hat{\mathbf{x}}_j^f(t+\delta)) \tag{26}$$

where $\hat{\mathbf{x}}_j^f(t+\delta)$ is obtained by running the model forward in time over $\delta = 12$ h with the unfiltered state $\mathbf{x}_j^a(t)$ as initial condition. The filtered analysis $\langle \mathbf{x}_j^a(t) \rangle$ becomes the initial condition for the ensemble forecast $\mathbf{x}_j^f(t+\delta)$. The recursive filter described in (26) correspond to a three point moving average, centered in time.

5. Results of LaDA

The three sequential methods (EuDA, LaDA2d and LaDA3d) are started with the same initial conditions (see the three left panels from the top row of Fig. 2). The maximum sample standard deviation of the layer thicknesses and velocities calculated from the ensemble for the case of LaDA2d is depicted in Fig. 6. It decreases rapidly to an asymptotic value after about 5 days, this is shown in the layer thicknesses and in the velocities of the second and third layer. The spread of the velocity of the top layer does not seem to have a clear asymptotic behavior over the span of the assimilation (50 days).

EuDA fails to recreate the eddy shedding and its propagation, but the two LaDA methods recreate the eddy after less than 10 days of assimilation. Since we are mostly interested in the estimation of the eddy-shedding process and the eddy-propagation process, the RMS errors from the three different cases are computed within a 250 km radius from the center of the eddy. The localized RMS errors between the thickness of the three layers are depicted in Fig. 7. The error of LaDA3d (solid line of Fig. 7) converges faster than that of LaDA2d (dashed line of Fig. 7). The two LaDA methods predict well the layer thicknesses and converge to the truth.

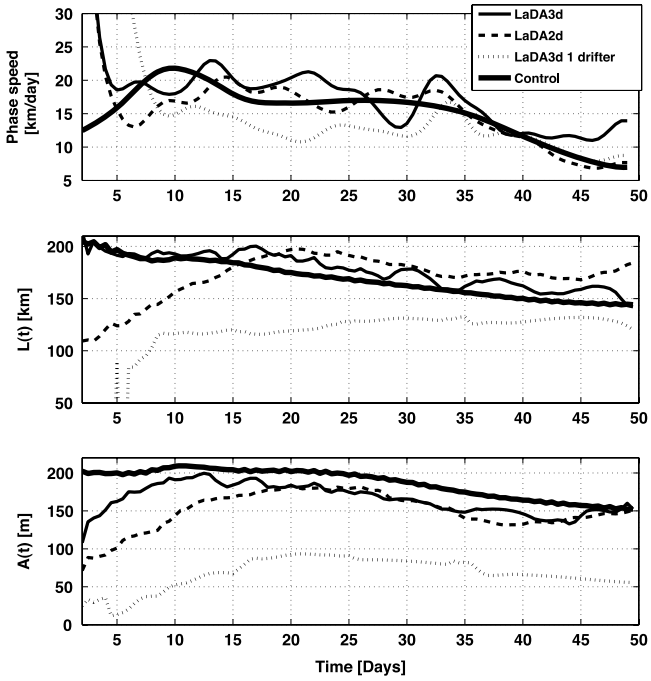

Fig. 10. Parameters of the eddy; LaDA2d (thin solid), LaDA3d (dashed), LaDA3d with one isopycnal float (dotted) and truth (thick solid). Top panel: Estimated phase speed between the analysed phase speed and true phase speed; Middle panel: $L(t)$; Bottom panel: Parameter $A(t)$.

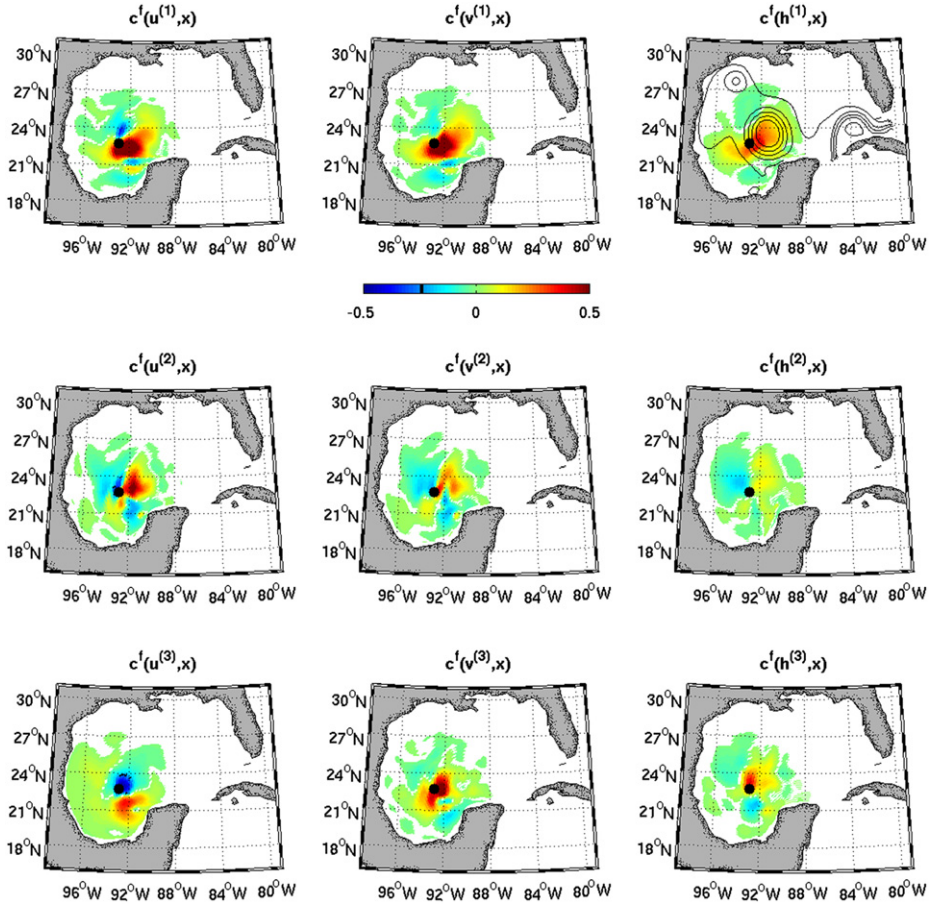

Fig. 11. Correlation function corresponding to the observation of the zonal position of a drifter at 25 days. The black dot is the observed position of the drifter. The top panel is the top layer, middle panel correspond to layer 2 and the bottom panel corresponds to layer 3. Contours of SSH are shown in the right-most upper panel.

In the following, we investigate the effectiveness of the three methods for the eddy-propagation process. In this work, the eddy center, diameter and amplitude are determined by fitting a Gaussian shaped function to the computed top layer thickness field. This method is

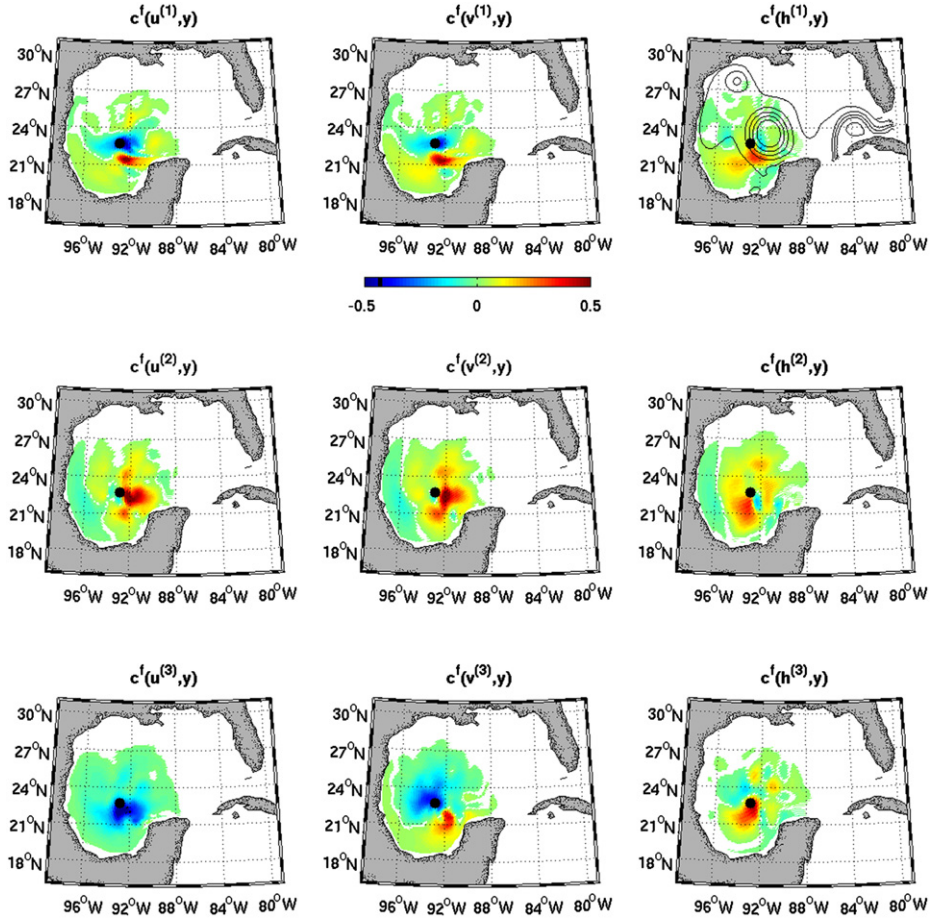

Fig. 12. Same as Fig. 11 but for the meridional position of a drifter at 25 h.

similar to that of Challenor et al. [27]. The reader is referred to [28], who tracked eddies by following the closed contour of the Okubo–Weiss parameter.

The parameters representing the eddy are obtained by minimizing,

$$\mathcal{J}(\alpha, \beta, L, A, B, t) = \iint_{\Omega} \left(A \exp\left(-\left(\frac{x-\alpha}{L}\right)^2 - \left(\frac{y-\beta}{L}\right)^2 \right) + B - h^{(1)}(x, y, t) \right)^2 \mathrm{d}x\mathrm{d}y \tag{27}$$

every 12 h. $\Omega = \{(x, y) \parallel (x-\alpha)^2 + (y-\beta)^2 < L_0^2\}$ is a disc of radius $L_0 = 250$ km centered at the location (α, β) of the center of the eddy. The functional (27) is minimized for the case of the control run and the analysis steps of the three data assimilation methods. The trajectory of the eddy is then interpreted as the center of the Gaussian shape, (α, β), and its radius and intensity are directly related to the parameters L and A, respectively. To justify the use of such a simple function, Fig. 8 depicts a snapshot of the proximity between the Gaussian shaped function and the eddy from the control run at 43 days. The surface is the Gaussian shape and the black dots represent the true top layer thickness.

As depicted in Fig. 9, the two LaDA methods are predicting the eddy center fairly well, with the LaDA3d case predicting a better track. The EuDA fails to estimate the correct position of the eddy. After the 50 days of integration, the two Lagrangian methods are similar in performance: they both give estimates of the parameters A and L close to the truth (see Fig. 10). The same behavior is observed in the phase speed (computed from the trajectory of the eddy). On the other hand, the LaDA3d converges faster (about 15 days) than the LaDA2d, this is seen clearly in the time series of the parameter A and L, shown in Fig. 10.

A similar experiment, assimilating only one isopycnal float, also recovered the eddy statistics fairly well. The eddy trajectory is depicted as the thin dotted line of Fig. 10. The propagation speed of the eddy is recovered with reasonable accuracy, because the float moves with the eddy, but the amplitude and the radius are underestimated.

6. Structure of the correlation function

In this section, we investigate the spatial structure of the scaled representers or correlation function. They are defined as the estimate of the correlations between the model's state variables and the observations. A representer defines the influence that an observation will have on the state after assimilation. The investigation of the geometrical structure and extent of influence of the representers are therefore crucial for understanding the effect that the observations have on the analysis and guide us in refining the assimilation scheme.

The correlation matrix, of which the columns correspond to the discrete form of the correlation function, is defined as in (23) but with $\mathbf{x}_D$ being one of the three types of observations: the surface velocity at fixed point for the EuDA, the meridional and zonal position of a surface

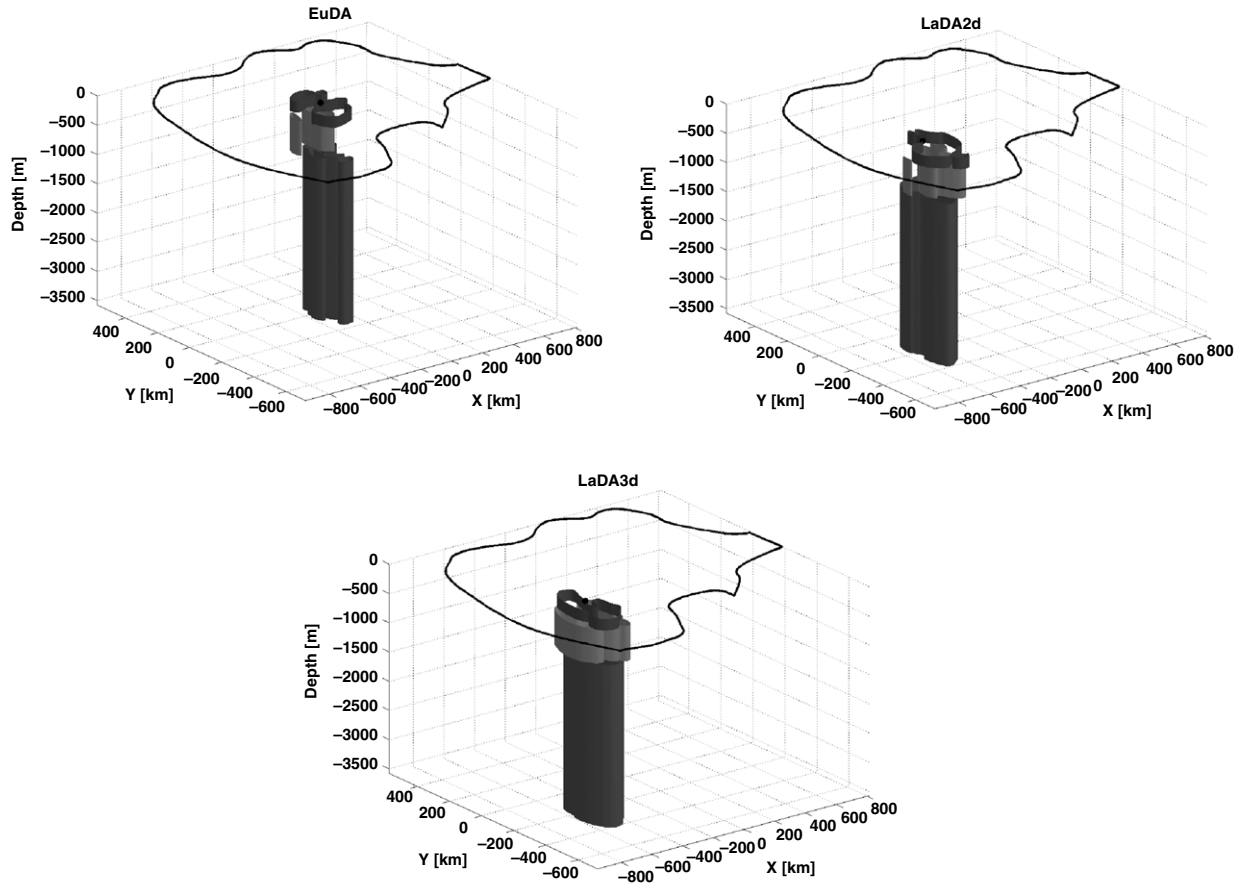

Fig. 13. Volumes of influence, as defined in (28). The gray surfaces are the boundaries of the RI. From top to bottom, $\mathcal{R}_{\text{EuDA}}$, $\mathcal{R}_{\text{LaDA2d}}$ and $\mathcal{R}_{\text{LaDA3d}}$. The thick black dots represents the horizontal position of the observing device. On the bottom panel, the position of the isopycnal float, has been projected onto the surface.

drifter for the LaDA2d or the three-dimensional position of the isopycnal float for the LaDA3d. In the case of LaDA2d, each odd (even) column of the $N \times L$ matrix $\mathbf{C}_{FD}$ represents the correlation between the state $\mathbf{x}_F^f$ of the ocean model and the observed meridional (zonal) coordinate of the float's discrete trajectory at the time of the observation. An example of the two correlation functions corresponding to the observed meridional and zonal position of a drifter in the LaDA2d case, after 25 days of assimilation are shown in Figs. 11 and 12. The colors represent the correlations between the state and the meridional or zonal position of the drifter. As expected, the maximum correlation for both representers are localized around the position of the drifter and are larger in the top layer than in the bottom layers. The correlation between $h^{(1)}$ and longitudinal position of the drifter, denoted as $c^f(h^{(1)}, x)$ in Fig. 11 shows an extremum just east of the location of the observation.

In a manner similar to [23], we introduce the notion of region of influence (RI). For individual observing device, we define the RI

$$\mathcal{R}_l^f = \{(x, y, z) | c_{\max}^f > c_{\text{ref}}\} \tag{28}$$

where $c_{\max}^f$ is the maximum of $(\mathbf{C}_{FD}^f)^{ij}$ at each grid point with i corresponding to the model variables at the grid point and j corresponding to the observation variables of the l-th observing device. We also define the total RI as the union of $\mathcal{R}_l^f$ of all the observing devices for LaDA2d, LaDA3d and EuDA, respectively. We define the surface of influence $\partial\mathcal{R}^f$ as the boundary of $\mathcal{R}^f$. Snapshots of $\partial\mathcal{R}^f$ for the three types of observations after 25 days of assimilation are depicted in Fig. 13. They extend over the three active layers of the model, implying that Lagrangian observations of the upper water column will have an effect on the lower part of the water column. This approach enables us to quantify how far the dynamical information contained in the observation can reach, and compare the efficiency of assimilating different type of observations. We define $\mathcal{V}_{\text{EuDA}}^f$ as being the volume of $\mathcal{R}_{\text{EuDA}}^f$, $\mathcal{V}_{\text{LaDA2d}}^f$ is the volume of $\mathcal{R}_{\text{LaDA2d}}^f$, and $\mathcal{V}_{\text{LaDA3d}}^f$ is the volume of $\mathcal{R}_{\text{LaDA3d}}^f$. These volumes are computed using the mean layer thicknesses as the height of the cylinders and the area defined by the boundary of the $\partial\mathcal{R}^f$. The probability density function of the volumes is obtained from the set of volume computed sequentially during 50 days for the three types of data. The total size of each set is 396 and the bin size is set to 40. Although the shapes of these distributions are complex Fig. 14, they reflect the idea that more observations result in larger volumes. Table 1 shows that the expected value of the volume of the RI for each layers and for the three different type of observations. For all layers, we have,

$$\text{E}(\mathcal{V}_{\text{EuDA}}^f) < \text{E}(\mathcal{V}_{\text{LaDA2d}}^f) < \text{E}(\mathcal{V}_{\text{LaDA3d}}^f). \tag{29}$$

The typical horizontal scales for these volumes ranges from 142 km for EuDA to 277 km for LaDA3d.

We define a measure of the amount of dynamical information gathered by the observing system in the following way:

$$\theta^{(j)2} = \sum_{i=1}^{L} \|c^f(u^{(j)}(x, y), \mathbf{x}_D^{(i)})\|^2 + \|c^f(v^{(j)}(x, y), \mathbf{x}_D^{(i)})\|^2 + \|c^f(h^{(j)}(x, y), \mathbf{x}_D^{(i)})\|^2 \tag{30}$$

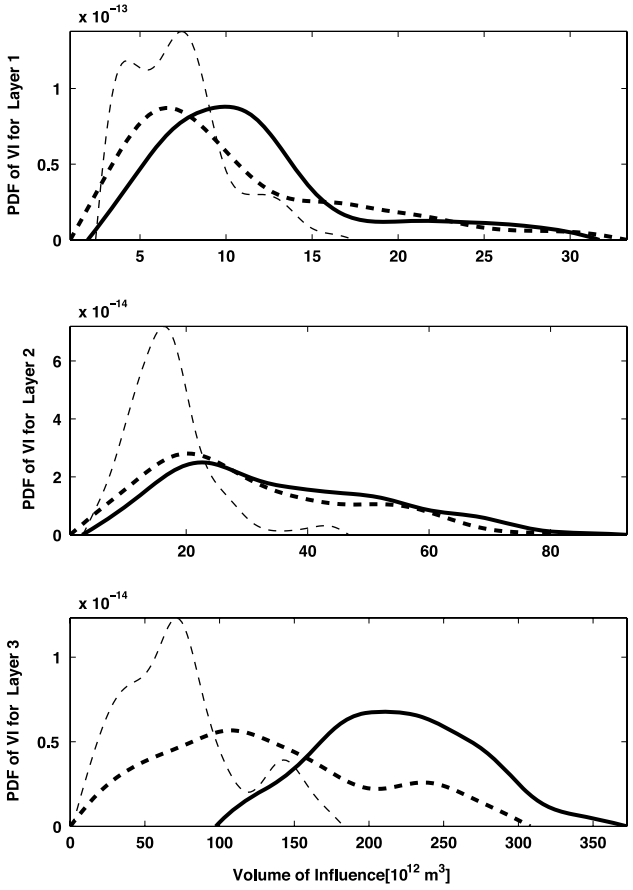

Fig. 14. Probability distribution functions for the volumes: $\mathcal{R}_{\text{EuDA}}$, $\mathcal{R}_{\text{LaDA2d}}$, $\mathcal{R}_{\text{LaDA3d}}$. The thin dashed line correspond to EuDA, the thick dashed line correspond to LaDA2d and the thick line correspond to LaDA3d.

Table 1
Expected value of the volume of influence for each layer in 10^{13} m^3.

	$E(\mathcal{V}_{\text{EuDA}})$	$E(\mathcal{V}_{\text{LaDA2D}})$	$E(\mathcal{V}_{\text{LaDA3D}})$
Layer 1	0.67	1.03	1.14
Layer 2	1.63	2.96	3.48
Layer 3	7.2	12.87	21.53

for $(x, y) \in \Omega$, where $\theta^{(j)}$ is the norm of the correlation function between the observing system and the model's variables in layer j. The norm $\|.\|$ is defined as,

$$\|f\|^2 = \frac{1}{\pi L_0^2} \iint_{\Omega} f^2 \mathrm{d}x\mathrm{d}y \tag{31}$$

where f is a function in the plane. A large value for θ is well correlated with a fast convergence to the truth and a small RMS error for the two top layers, this can be observed by comparing the two top panels of Figs. 15 and 7. This is however not true for the bottom layer where $\theta^{(3)}_{\text{LaDA2d}} < \theta^{(3)}_{\text{LaDA3d}}$ but LaDA3d is not performing significantly better than LaDA2d (see the bottom panel of Fig. 15). For LaDA3d, the contribution to the amount of dynamical information available from observing $h^{(1)}$ is shown as the difference between the thin and thick solid lines in Fig. 15. The thin line denoted as LaDA3d no $h^{(1)}$ in Fig. 15 was computed by setting the correlation between the state and the observation of the depth, $h^{(1)}$, to zero. The contribution is significant at all times, but is only beneficial at reducing the RMS at the beginning of the assimilation and only for the top two layers. The relative error in total kinetic energy between the analysis and the truth for layer j is defined as:

$$\mathcal{E}^{(j)} = \frac{\iint_{\Omega} ({u^{(j)}}^2 + {v^{(j)}}^2)\mathrm{d}x\mathrm{d}y - \iint_{\Omega} ({u_t^{(j)}}^2 + {v_t^{(j)}}^2)\mathrm{d}x\mathrm{d}y}{\iint_{\Omega} ({u_t^{(j)}}^2 + {v_t^{(j)}}^2)\mathrm{d}x\mathrm{d}y} \tag{32}$$

where $(u^{(j)}, v^{(j)})$ are the velocities from EuDA, LaDA2d or LaDA3d. The slow convergence to the truth, observed in the bottom layer RMS, is attributed to the two LaDA method introducing too much kinetic energy in the bottom layer (see Fig. 16) at the beginning of the assimilation.

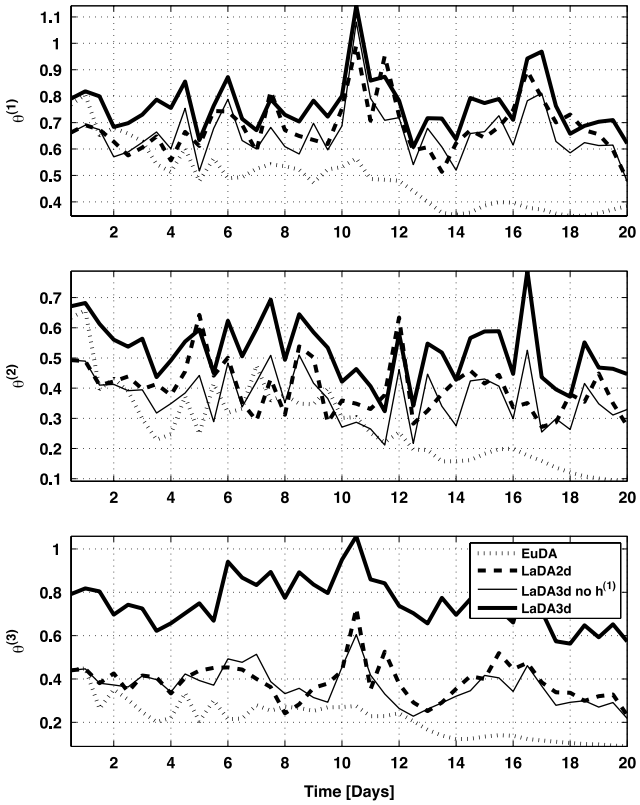

Fig. 15. Norm of the correlation function for the three layers.

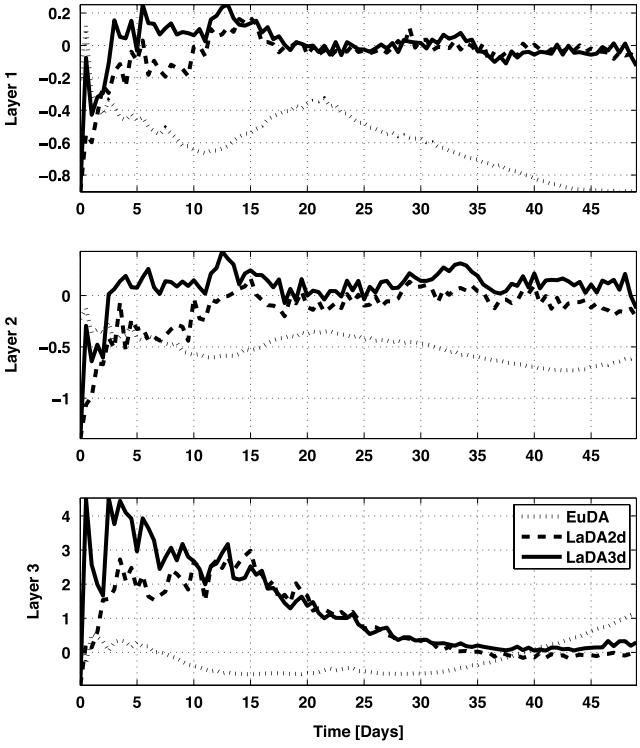

Fig. 16. Relative error in kinetic energy for the three layers.

7. Discussion

We have assimilated three types of observations, namely, the measurement of velocities at fixed station, the horizontal positions of surface drifters, and the three-dimensional positions of isopycnal floats. We have shown that only the two LaDA methods where capable of reproducing the eddy-shedding process and that even only one carefully placed isopycnal float can lead to a reasonable estimation of the

eddy-shedding process. A poorly chosen launching position would result in the drifter sampling a region that contains little information about the eddy. This is exactly what happens in the case of the fixed station where information about the eddy is sampled for a very brief period of time. The remarkable efficiency of LaDA was investigated by looking at the structure and properties of the correlation functions. Lagrangian regions of influence (RI) were defined and compared to the corresponding regions arising from assimilating Eulerian observations. The two Lagrangian RI's were found to be significantly larger than the Eulerian one, with the RI for LaDA3d being the largest of the three. The efficiency of the assimilation method is related to these RI and the corresponding norm of the correlation function. The analysis of the correlation function did not explain the similar performance of the LaDA2d and LaDA3d for the bottom layer, where the RI for LaDA3d is larger than the RI for LaDA2d but the RMS of both methods are similar.

As opposed to the RI arising from Eulerian observation at fixed stations, the RI of Lagrangian observation can be maximized by choosing a set of trajectories that will track the information of interest. In the case of this study, following the eddy. A method describing the choice of trajectories while only knowing an a priori flow field is proposed in [15,16]. The method is based on the analysis of the Lagrangian coherent structure of the flow and is a first step toward addressing the problem of launching position.

It is of course more challenging in the case of a realistic assimilation system. One would be assimilating noisy drifter positions sampled from an ocean that significantly differ from a modeled ocean that not only has simplified physics but also contains biases. For example, an observed trajectory would have information about small scales turbulent flow that the model cannot resolve, or a loop current that the model constantly predicts to be further north or south than the observed current. Although these problems were not addressed in this paper, from what we have learned from this work, we believe that our method would also work in the case of real observation and a more complex ocean model.

Acknowledgements

The research of Kayo Ide was supported by the Office of Naval Research under grant number N000140910418. The research of Guillame Vernieres and Christopher Jones was supported by the Office of Naval research under grants N000140910986 and N000140910235.

References

[1] J. Ochoa, A.B. Sheinbaum, J. Candela, D. Wilson, Geostrophy via potential vorticity inversion in the yucatan channel, J. Mar. Res. 59 (2001) 725–747.
[2] L.Y. Oey, T. Ezer, D.P. Wang, Loop current warming by hurricane wilma, Geophys. Res. Lett., 33 L08613.
[3] K. Ide, L. Kuznetsov, C.K.R.T. Jones, Lagrangian data assimilation for point-vortex system, J. Turbul. 3 (2002) 53.
[4] L. Kuznetsov, K. Ide, C.K.R.T. Jones, A method for assimilation of Lagrangian data, Mon. Weather Rev. 131 (10) (2003) 2247–2260.
[5] G. Evensen, Sequential data assimilation with a nonlinear quasi-geostrophic model using Monte Carlo methods to forecast error statistics, J. Geophys. Res. 99 (C5) (1994) 10143–10162.
[6] G. Evensen, P.J. van Leeuwen, An ensemble kalman smoother for nonlinear dynamics, Mon. Weather Rev. 128 (2000) 1852–1867.
[7] G. Evensen, The ensemble kalman filter: theoretical formulation and practical implementation, Ocean Dyn. 53 (2003) 343–367.
[8] H.E. Hurlburt, J.D. Thompson, A numerical study of loop current intrusions and eddy shedding, J. Phys. Oceanogr. 10 (1980) 1611–1651.
[9] J.F. Thompson, Z. Warsi, C.W. Martin, Numerical Grid Generation Foundation and Applications, North-Holland, 1985.
[10] J.E. Castillo (Ed.), Mathematical Aspect of Numerical Grid Generation, SIAM, 1991.
[11] R. Courant, D. Hilbert, Methods of Mathematical Physics, Wiley Interscience, New York, 1962.
[12] R.D. Richtmyer, K.W. Morton, Difference Methods for Initial-Value Problems, Interscience Publishers, New York, 1967.
[13] M. Xue, High-order monotonic numerical diffusion and smoothing, Mon. Weather Rev. 128 (1999) 2853–2864.
[14] F. Schott, T. Lee, R. Zantopp, Variability of structure and transport of the florida current in the period range of days to seasonal, J. Phys. Oceanogr. 18 (1988) 1209–1230.
[15] H. Salman, L. Kuznetsov, C.K.R.T. Jones, K. Ide, A method for assimilating Lagrangian data into a shallow-water equation ocean model, Mon. Weather Rev. 134 (10) (2006) 1081–1101.
[16] H. Salman, K. Ide, C.K.R.T. Jones, Using flow geometry for drifter deployment in Lagrangian data assimilation, Tellus 60 (2) (2008) 321–335.
[17] K. Ide, P. Courtier, M. Ghil, A. Lorenc, Unified notation for data assimilation: operational, sequential and variational, J. Meteorol. Soc. Japan 75 (1997) 181–189.
[18] A.F. Bennett, B.S. Chua, L.M. Leslie, Generalized inversion of a global numerical weather prediction model, II: analysis and implementation, Meteor. Atmos. Phys. 62 (1997) 129–140.
[19] B.S. Chua, A.F. Bennett, An inverse ocean modeling system, Ocean Modell. 3 (2001) 137–165.
[20] A.F. Bennet, Inverse Modeling of the Ocean and Atmosphere, Cambridge University Press, Cambridge, 2002.
[21] Gerrit Burgers, Peter Jan van Leeuwen, Geir Evensen, On the analysis scheme in the ensemble Kalman filter, Mon. Weather Rev. 126 (1998) 1719–1724.
[22] X.-Q. Yin, L.-Y. Oey, Bred-ensemble ocean forecast of loop current and rings, Ocean Modell. 17 (4) (2007) 300–326.
[23] E.F. Carter, Assimilation of Lagrangian data into a numerical model, Dyn. Atmos. Oceans 13 (1989) 335–348.
[24] J.L. Mead, A.F. Bennett, Towards regional assimilation of Lagrangian data: the Lagrangian form of the shallow water model and its inverse, J. Mar. Syst. 29 (2001) 365–384.
[25] F. van Hees, A.J. van der Steen, P.J. van Leeuwen, A parallel data assimilation model for oceanographic observations, Concurr. Comput.: Pract. Exp. 15 (2001) 1191–1204.
[26] P.L. Houtekamer, H.L. Mitchell, A sequential ensemble kalman filter for atmospheric data assimilation, Mon. Weather Rev. 129 (2001) 123–137.
[27] P.G. Challenor, P. Cipollini, D. Cromwell, Use of the 3-D radon transform to examine the properties of oceanic rossby waves, J. Atmos. Oceanic Technol. 18 (9) (2001) 1558–1566.
[28] D.B. Chelton, M.G. Schlax, R.M. Samelson, R.A. de Szoeke, Global observations of large ocean eddies, Geophys. Res. Lett. 34 (2007), L15606. doi:10.1029/2007GL030812.